Nature Geoscience
DOI: 10.1038/ngeo1639

Importance of density-compensated temperature change for deep North Atlantic Ocean heat uptake

C. Mauritzen · A. Melsom · R. T. Sutton

Received 5 July 2012; accepted 22 October 2012

The efficiency with which the oceans take up heat has a significant influence on the rate of global warming. Warming of the ocean above 700 m over the past few decades has been well documented. However, most of the ocean lies below 700 m. Here we analyse observations of heat uptake into the deep North Atlantic. We find that the extratropical North Atlantic as a whole warmed by $1.45 \pm 0.5 \cdot 10^{22}$ J between 1955 and 2005, but Lower North Atlantic Deep Water cooled, most likely as an adjustment from an early twentieth-century warm period. In contrast, the heat content of Upper North Atlantic Deep Water exhibited strong decadal variability. We demonstrate and quantify the importance of density-compensated temperature anomalies for long-term heat uptake into the deep North Atlantic. These anomalies form in the subpolar gyre and propagate equatorwards. High salinity in the subpolar gyre is a key requirement for this mechanism. In the past 50 years, suitable conditions have occurred only twice: first during the 1960s and again during the past decade. We conclude that heat uptake through density-compensated temperature anomalies will contribute to deep ocean heat uptake in the near term. In the longer term, the importance of this mechanism will be determined by competition between the multiple processes that influence subpolar gyre salinity in a changing climate.

C. Mauritzen
Norwegian Meteorological Institute, P.O. Box 43 Blindern, NO-0313 Oslo, Norway.
E-mail: c.mauritzen@cicero.uio.no
Present address: CICERO Center for International Climate and Environmental Research, NO-0318 Oslo, Norway

A. Melsom
Norwegian Meteorological Institute, P.O. Box 43 Blindern, NO-0313 Oslo, Norway

R. T. Sutton
National Centre for Atmospheric Science, University of Reading, Reading RG6 6BB, UK

The rate of global warming is determined by changes in the radiative forcing of the Earth system, due to increasing greenhouse gases and other factors, and by Earth's heat capacity, which is dominated by that of the oceans[1,2]. The recent warming of the upper ocean, above 700 m, is well established[3–5]. However, here our focus is the deep ocean: if substantial quantities of heat can penetrate below 700 m, this would increase the effective heat capacity of the Earth system, and could potentially slow global warming. There is now evidence that, between the 1990s and 2000s, there were significant increases in global ocean heat storage below 4.000 m, stemming from the Southern Ocean[6]. Deep warming can also make important contributions to sea level rise[2,6–8]. Understanding the role of deep waters in ocean heat uptake is therefore a critical and urgent challenge.

Two issues make understanding heat uptake by the deep ocean difficult. First, is the lack of observations. The deep ocean is poorly observed, and there is a particular lack of consistent multidecadal records, which are needed to identify climatically important trends against the background of natural variability. Second, there is an incomplete understanding and quantification of the processes involved. In this study we focus, following ref. 9, on the role of the deep North Atlantic Ocean, which is the best sampled of all the world's ocean basins, and also host to one of the few regions where the deep ocean is efficiently ventilated from the surface. On average, 15 – 20 million cubic metres of wa-

ter are transferred from the surface to the deep ocean every second in the North Atlantic[10–12], playing a key role in the global overturning circulation. On the other hand, this region is well known for being strongly influenced by atmospheric modes of variability (notably, the North Atlantic Oscillation, NAO)[13–15], making identification of long-term trends particularly difficult. Our aim is to characterize, quantify and understand the role of the deep North Atlantic Ocean in heat uptake over the past 50 years, and to assess what lessons can be learned for future projections. We focus on temperature changes within specific water masses—in particular Upper and Lower North Atlantic Deep Water. Although the data are sparse, we demonstrate that—when analysed in water mass space—they show broad, coherent signals in the deep ocean. In the long-term mean, the temperature structure of a limited region of the World Ocean, such as the North Atlantic, is determined by a balance between the downward mixing of heat from warm surface regions by isopycnal and diapycnal diffusion, formation and sinking of cold dense waters at high latitudes[16], and exchanges of water with the rest of the global deep oceans. There are two dimensions of change in deep water formation that can perturb this equilibrium state: changes in the formation rate and changes in the hydrographic properties (temperature, T, and salinity, S) of the newly formed water[17]. Changes in temperature and salinity may also arise from vertical displacement of isopycnals (heave), caused by dynamical processes such as the response to variations in wind stress curl[17] and from horizontal advection. Often changes to T and S involve only insignificant changes in density or volume. Such density-compensated T and S anomalies have no direct influence on ocean circulation or sea level, but can be associated with substantial variations in heat content. In contrast, uncompensated T and S anomalies are directly related to anomalies in density, and hence circulation. Previous studies have shown a high level of T—S compensation in the decadal variability of dense water formed in the North Atlantic, specifically in the Labrador Sea Water[18–22]. However, as the authors of these studies point out, the changes are not fully density compensating. A specific aim of our study is to identify and quantify the roles of compensated and uncompensated temperature variations for heat uptake by the deep North Atlantic Ocean.

The study is based on new analyses of 5-year (pentadal) mean anomalies of temperature and salinity from 1955 to 2005 (see **Methods**). According to this data set the total heat content in the extratropical North Atlantic Ocean (between 20°N and the Greenland–Scotland Ridge) has increased by $1.45 \pm 0.5 \cdot 10^{22}$ J since 1955 (thick solid line in Fig. 1 a), equivalent to an average anomalous downward heat flux of $0.4\,\mathrm{Wm}^{-2}$ through the sea surface of this region, consistent with previous North Atlantic estimates[9,23]. Whereas the full water column shows a positive trend with decadal variations superposed, the upper 700 m shows some cooling until the mid-1980s, and, since then, rapid warming. Below 2.000 m the North Atlantic has cooled significantly in recent decades (Fig. 1 a and Suppl. Tbl. S1).

Analysis in density space

To elucidate the processes underlying these changes in heat content we divide the water column into the primary water masses of the North Atlantic: the thermocline waters, or Central Waters, or warm water zone ($\sigma_1 < 32.15$); the Upper North Atlantic Deep Water (UNADW; $\sigma_1 > 32.15$ and $\sigma_2 < 37.0$), originating in the Subpolar Gyre (SPG); the Lower North Atlantic Deep Water (LNADW; $\sigma_2 > 37.0$ and $\sigma_4 < 45.9$), originating north of the Greenland–Scotland Ridge; and, towards the bottom, modified Antarctic Bottom Water (mAABW); see details in Suppl. Fig. S3 and Suppl. Tbl. S2. Energy changes within a water mass defined in density space can arise from changes in its mean temperature or from changes in its volume. For our first analysis we eliminate changes in volume by using the 50-year climatological position of the water mass interfaces, and calculate heat content changes within the water masses (Fig. 1 b–f; note that time series of water mass volume anomalies are shown in Suppl. Fig. S4). A notable feature of Fig. 1 b is the contrasting behaviour of Upper and Lower NADW: UNADW heat content shows a rapid increase during the 1960s and a rapid decline during the 1980s and 1990s, whereas LNADW heat content shows a steady decline from the 1970s. Overall, the deep water masses have lost, rather than gained, heat during the past 50 years (Fig. 1 b): between 1955 and 2005 the net heat loss of LNADW was $4.3 \pm 0.5 \cdot 10^{21}$ J; meanwhile, UNADW gained only $2.9 \pm 1.3 \cdot 10^{21}$ J (and note that the variability of UNADW heat content is much larger than this net change, which is a simple subtraction of the first pentad from the last).

We further partition the North Atlantic into the subtropical gyre (STG; 20 and 50°N) and the SPG (50°N to the Greenland–Scotland Ridge) subdomains (Fig. 1c,d). Three fifths of the total warming since 1955 ($0.9 \pm 0.5 \cdot 10^{22}$ J) has occurred in the STG (Fig. 1 c, thick line); the remaining two fifths ($0.6 \pm 0.1 \cdot 10^{22}$ J) has occurred in the SPG (Fig. 1 d, thick line). The imprint of the NAO on the total (top-to-bottom) heat content is clear: the persistent low NAO index of the 1960s resulted in anomalously high heat content in the SPG (Fig. 1 d, thick line), whereas the persistent high

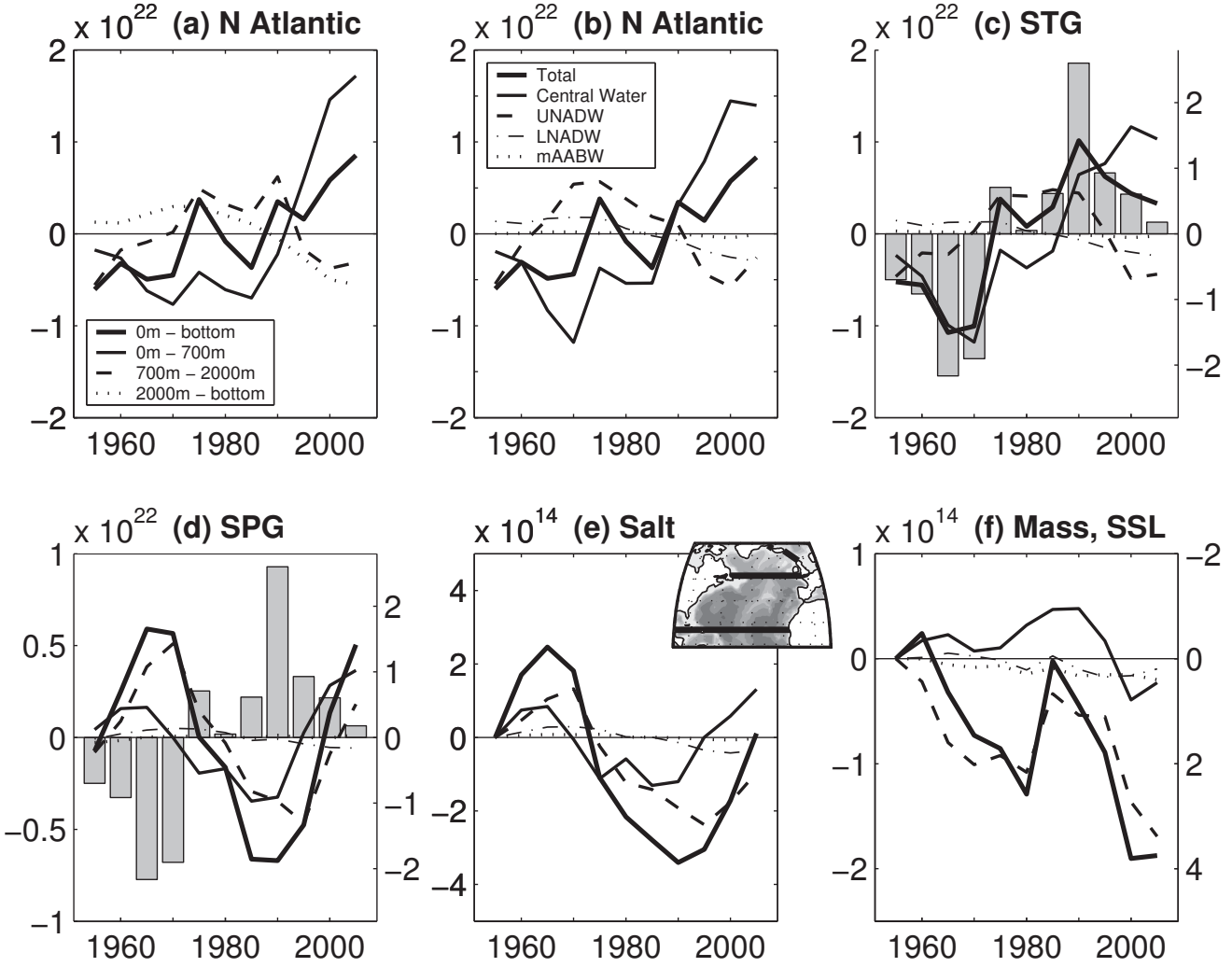

Figure 1 — Heat content changes (J) in the extratropical North Atlantic between 1955 and 2005. Changes in the extratropical North Atlantic, in depth layers (**a**) and within the water masses defined in the text (**b**) calculated between the climatological (1955–2005) average position of each water mass interface. **c**, The same as in **b**, but for the STG. **d**, The same as in **b**, but for the SPG. **e**, The same as in **d**, but for salt (kg). **f**, The same as in **d**, but for mass (kg). In **f**, the curve Total is also given as steric sea level (SSL) anomaly (right-hand axis, inverted, (cm)). For **a-d** the anomalies are relative to the average value for each time series, whereas for **e** and **f** the anomalies are offsets from the 1953 to 1957 pentad. Uncertainties are given in Suppl. Tbl. S3; generally in **b-d** they range $0.5 - 2 \cdot 10^{21}$ J for Central Water and UNADW, and the LNADW is $0.4 \cdot 10^{21}$ J. For these three water masses, the uncertainty is typically $1 \cdot 10^{13}$ kg in **e** and **f**. Also shown (**c,d**; bars; scale on right-hand side) is the winter NAO index, defined as the December–March station-based index, relative to the 1953–2007 mean[42]. Inset, a map of the region.

NAO index of the late 1980s and early 1990s resulted in anomalously low heat content, as reported by numerous authors[9,24,25]. In the STG, the evolution is the opposite: superimposed on the warming trend there is a distinct low in heat content in the 1960s and a high around 1990 (Fig. 1 c, thick line). This contrast between the SPG and STG was recognized in ref.s 13 and 9 and explained as primarily due to the change in buoyancy forcing in the case of the SPG, and primarily due to the change in wind forcing in the case of the STG (ref. 9). We will add a minor twist to this explanation further below.

In the SPG (Fig. 1 d) maxima in heat content appear first at the surface (in the Central Waters), and then subsequently in the UNADW and LNADW, with a time lag of 5–10 years. The variations in LNADW heat content are much smaller than those in the water masses above, a finding that is consistent with the relative stability of the properties of the Overflow Waters (which feed the LNADW), compared with the highly variable UNADW (see, for example, Fig. 6a in ref. 20). In the STG (Fig. 1 c) only the Central Waters are exposed to the sea surface; they show a cooling in the 1960s, followed by a warming trend. The evolution of

the deep waters is very different. Similarly to the North Atlantic as a whole (Fig. 1 b), UNADW shows a rapid increase in the 1960s, reaching a peak in the 1980s, followed by a rapid decline in the 1990s. LNADW heat content shows a steady decline since the 1970s. mAABW heat content also shows a small cooling trend.

Passive advection and potential circulation changes

How can we understand the evolution of heat content in the STG deep waters? Export of NADW (notably, Labrador Sea Water) towards the Equator is well documented[14,18,26–28]. Bands of positive and negative potential temperature (θ) and salinity (S) anomalies that originated in the UNADW of the SPG during prolonged low and high NAO periods (Fig. 1 d) propagate southwards into the STG on decadal timescales (Fig. 2 a,b) as noted by, for example, ref.s 14,29. Thus, the variations in UNADW heat content seen in the subtropics (Fig. 1 c) partly reflect a delayed response to the variations in the SPG a decade or two earlier. Coincidentally, the propagation timescale from the SPG to the STG is comparable to the main NAO timescale during the past five decades, such that by the time one anomaly reached the subtropics, an anomaly of the opposite sign appeared in the SPG (Fig. 2 a). This concurrent timescale may enhance the opposing phase of the heat content in the SPG and STG in recent decades, as a small addition to the mechanism proposed by ref. 9.

The relative phase of the UNADW θ and S anomalies suggests density compensation. However, as already noted, the compensation is not perfect. High density in the SPG precedes both the warm anomaly formed in the 1960s and the cold anomaly formed in the 1980s and 1990s (Fig.s 1 f and 2 c). Figure 2 c reveals that even the density anomalies propagate southwards in UNADW similarly to the θ and S anomalies. For all three variables, the propagation speed ($O(1\,\mathrm{cm\,s^{-1}})$) is similar to that observed for passive tracers in the region[30], suggesting that the propagating heat content anomalies may be viewed as dynamically passive to some degree. However, there is strong published evidence of changes in North Atlantic Ocean circulation in recent decades, related to changes in the mid-depth density structure[14]. Moreover, it is to be expected that variations in subpolar density would affect the volumes of deep waters produced[20]; in fact, we do find a weak positive correlation between the mass (average density) of the SPG Central Water and the volume of SPG UNADW ($r = 0.4 \pm 0.2$ after detrending). Variations in the volume of UNADW are revealed in layer thickness anomalies (Fig. 2 d). Particularly notable is the positive thickness anomaly that formed in the SPG during the high NAO years of the late 1980s and early 1990s

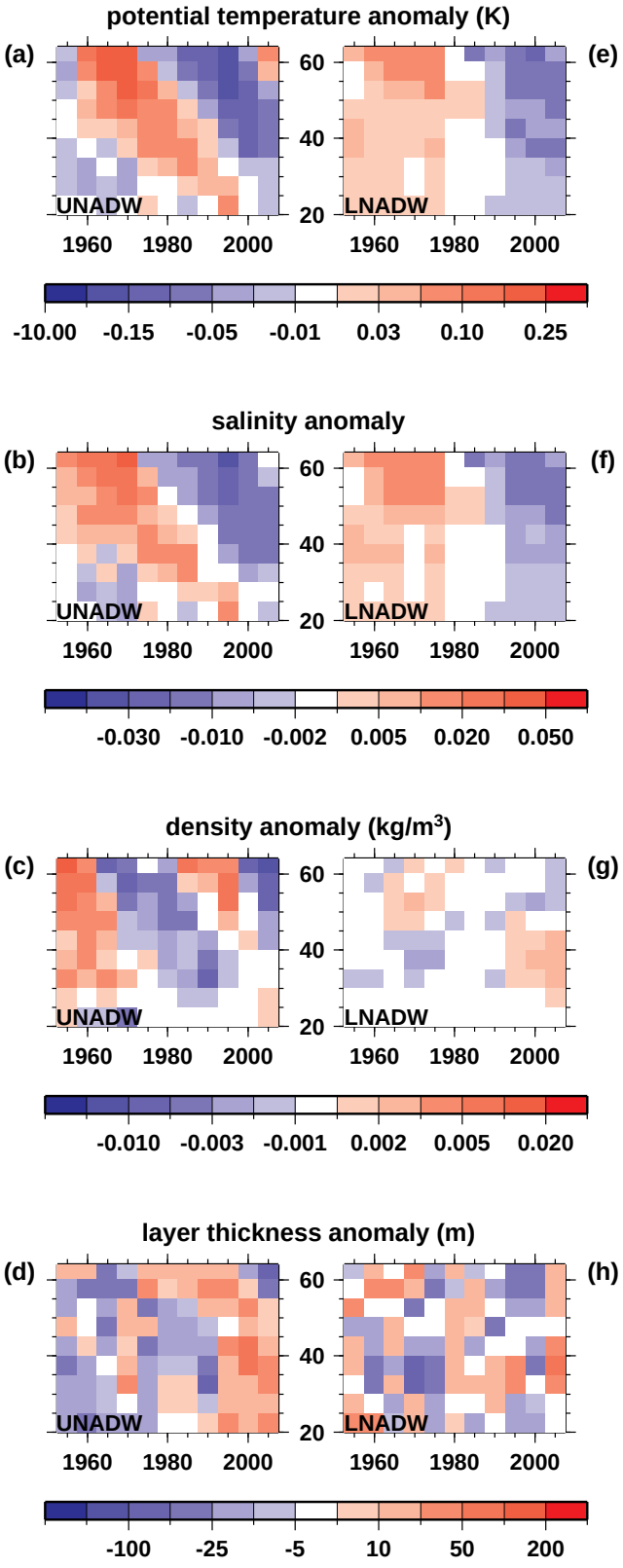

Figure 2 — Property anomalies, averaged vertically and zonally, within the NADW as a function of time and latitude. Potential temperature (°C; **a**,**e**), salinity (**b**,**f**), density ($\mathrm{kg\,m^{-3}}$; **c**,**g**) and thickness (m; **d**,**h**) anomalies for UNADW (left panels) and LNADW (right panels). The anomalies are created relative to the 1955–2005 mean. In the definition of the water mass interfaces we use here individual 5-year averages; however, using the 50-year climatology yields comparable results.

(Fig. 2 d), which may be linked to the positive thickness anomalies found subsequently, in the 1990s and 2000s, in the STG (same figure).

Short- and long-term transfer of heat to the deep ocean

The preceding analyses have indicated that both density compensation and dynamical changes in the large-scale circulation may be important for heat uptake in the deep North Atlantic. Although a heat budget can be calculated only for a fixed control volume, quantifying the magnitudes of energy changes for changing temperatures versus changing volumes of water masses (see **Methods**) is illuminating. We refer to this quantity as quasi-heat-content (QHC). The first contribution to QHC in the STG (Fig. 3) is closely related to the temperature anomalies shown in Fig. 2 a,e, and reflects changes in temperature that are compensated, when averaged over the layer, and therefore have no effect on the large-scale stratification and potential vorticity. Thus, we argue that this contribution may be viewed as passive from the point of view of large-scale ocean circulation, and that the persistence (or lifetime) of this contribution is likely to be comparable to that of passive tracers, that is, decades to centuries (determined by a combination of the timescales for NADW to upwell in the Southern Ocean, and for erosion by diapycnal mixing in the lower latitudes; timescales based on typical horizontal speeds and vertical diffusivities[16]). In contrast, the second contribution, which is closely related to the layer thickness anomalies shown in Fig. 2 d,h, is directly linked to changes in the large-scale stratification and potential vorticity. Thus, this contribution is active in relation to the large-scale ocean circulation. The persistence of this contribution will be directly linked to the persistence of the relevant changes in circulation; in the absence of catastrophic changes in circulation (for example, a shutdown of the Atlantic Meridional Overturning Circulation), it is likely to be much shorter than that of the passive contribution. In addition, because it is related to local mass divergence, the importance of the active contribution is likely to be much reduced in the global mean.

Focusing on the STG as the region where the key deep water masses are isolated from the atmosphere, we find that, for UNADW, variations in mean temperature and variations in volume have been of comparable importance over the past 50 years (Fig. 3 b). The temperature variations are dominated by the warm pulse that was exported from the SPG in the late 1970s/early 1980s, and the subsequent cool pulse, supporting our view that these anomalies are primarily passive with respect to the general circulation. The contribution from

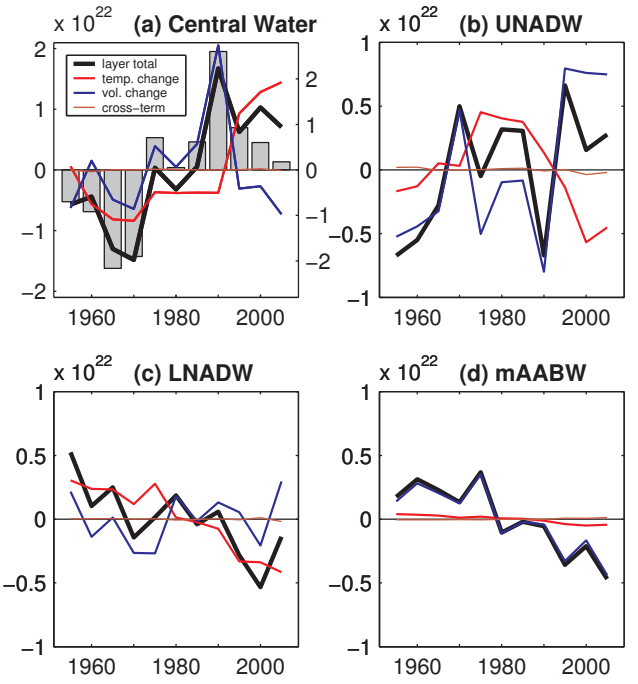

Figure 3 — Time series of QHC changes (J) within the four main water masses of the STG. a, CentralWater. **b**, UNADW. **c**, LNADW. **d**, mAABW. The uncertainties are given in Suppl. Tbl. S3; values are typically $1 \cdot 10^{21}$ J. Uncertainties in the cross-correlation terms are 1-2 orders of magnitude lower. Also shown is the winter NAO index (**a**; bars; scale on right-hand side), defined as the December-March station-based index, relative to the 1953–2007 mean[42].

volume is much noisier, owing to the many processes that can cause changes in isopycnal depth (planetary waves, eddies, tides and so on). Nevertheless, variations in the volume of UNADW are anticorrelated with variations in the volume of Central Waters ($r = 0.85 \pm 0.1$ after detrending) in the subtropics; this anticorrelation probably reflects—in substantial part—variations in thermocline depth due to changes in Ekman pumping/wind stress curl associated with changes in the NAO (ref. 9). We surmise that this wind-forced component of the variations in UNADW QHC is likely to be short-lived, with little enduring importance for ocean heat uptake. However, some variations in the volume contribution to the QHC may be related to more enduring aspects of circulation change. In particular, the large increase in the 1990s (Fig. 3 b), which is related to the thickness anomalies seen in Fig. 2 d discussed earlier, may be related to recent variations in the North Atlantic Overturning Circulation[22,31]. Overall, using this decomposition, taking into account both mean temperature and volume contributions, there was an increase in STG UNADW QHC of $0.9 \pm 0.3 \cdot 10^{22}$ J between 1955 and 2005, even though the change in mean temperature over this period was negative (Fig. 3 b).

Decadal variations in LNADW potential temperature and salinity are similar, in the SPG, to the variations seen in UNADW, although the amplitude is slightly less and there is a phase lag, relative to UNADW, of ∼ 5 years (Fig. 1 d,e). However, in the zonal mean (Fig. 2) the LNADW anomalies do not propagate into the subtropics like those in UNADW (contrast Fig.s 2 e,f and a,b). The spreading of the warm and cold pulses seems to stop at ∼ 45°N (Fig. 2 e), south of which a weaker cooling and freshening signal appears at all latitudes simultaneously (Fig. 2 e,f). Instead, the cold anomaly in the LNADW in the SPG in 1993–1997, for instance, (Fig. 4) spreads along the western rim, and no distinct anomaly develops in the basin interior (Fig. 4 g-j), explaining why the propagation signal is much less visible in the zonal average (Fig. 2 e). In contrast, the cold anomaly in the UNADW in the SPG in 1988–1992 spreads southwards both along the western rim and into the basin interior (Fig. 4 b-e), detected in Fig. 2 (and previously deduced from hydrography[26,32] and observed directly with RAFOS floats[33]). See Suppl. Fig.s S5 and S6 for the complete set of maps corresponding to Fig. 4.

Another key difference between the two water masses is that LNADW has generally been cooling since the beginning of the time series (Fig. 1 c), despite the warm pulse originating in the SPG in the 1970s (Fig. 1 d). Using our alternative decomposition (Fig. 3 c) we find that in contrast to UNADW, the change in QHC of LNADW in the STG is dominated by the mean temperature contribution, and specifically the cooling of this water mass, during the past 50 years (Fig. 3 c). Variations in volume contribute significant decadal variability but no net change. Whereas UNADW started from a fairly neutral state in the 1950s, LNADW started from an anomalously warm state (compare Fig. 4 a and f). This warm state of the LNADW in the 1950s and 60s may be a distant memory of the early twentieth-century warm period in the North Atlantic Ocean in the 1920s to 1940s (ref. 34).

Finally, the QHC reduction in mAABW throughout the period has been much larger than that expected from the temperature drop alone, owing to significant volume loss to the upper water masses (Fig. 3 d). A loss in the volume of mAABW from the 1980s to 2000s in the western North Atlantic has been reported by ref. 35. These authors found the volume loss to be associated with a reduced zonal gradient in abyssal temperatures, consistent with decreased northward transport ofmAABWinto our study area.

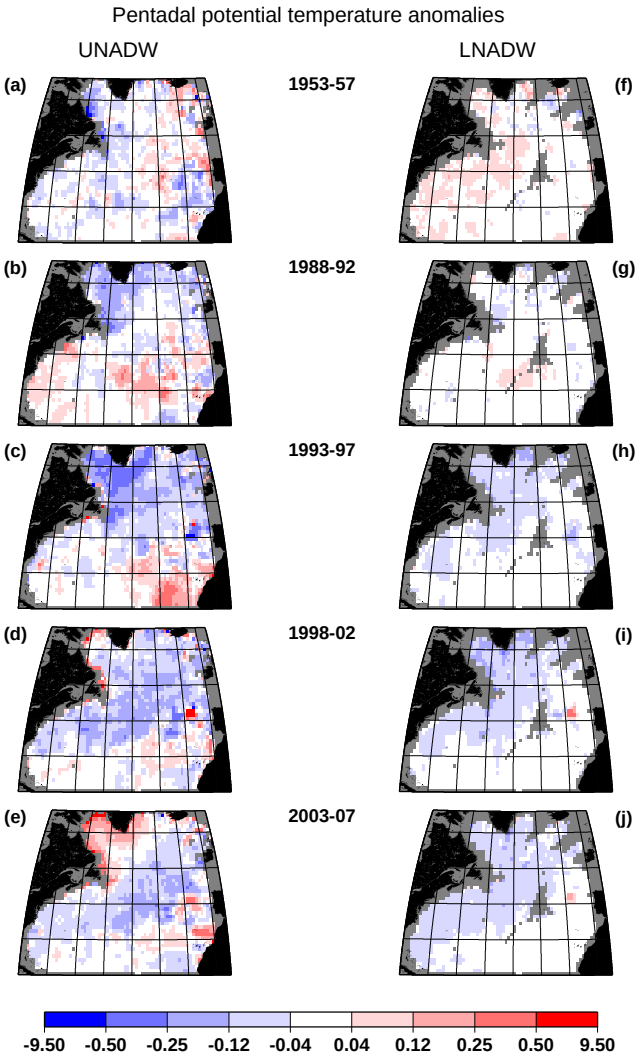

Figure 4 — Maps of depth-average temperature anomalies within UNADW and LNADW for selected 5-year periods. Maps for the pentads 1953–1957 (**a**,**f**), 1988–1992 (**b**,**g**), 1993–1997 (**c**,**h**), 1998–2002 (**d**,**i**) and 2003–2007 (**e**,**j**) for UNADW (left panels) and LNADW (right panels). The anomalies are created relative to the 1955–2005 mean. The water mass interfaces are here based on individual 5-year average data. The complete set of maps can be found in Suppl. Fig.s S5 and S6.

Future heat uptake by the compensated mechanism

A key conclusion of our study is that density-compensated temperature anomalies are very important for long-term heat uptake into the deep North Atlantic (Fig. 3). As we have argued already, these anomalies are likely to be characterized by a lifetime of decades to centuries. This conclusion highlights the need to understand the conditions under which suitable anomalies form—in particular warm, salty anomalies that increase ocean heat uptake. Only one such anomaly was formed during the period we have analysed: namely during the low NAO conditions of the 1960s. This anomaly was subsequently

exported into the subtropical UNADW layer. Thus, this mechanism for heat uptake by the deep North Atlantic is intermittent, and requires special conditions to be effective.

Upper ocean temperatures in the SPG are much higher at present than ever before in the record, and salinity has been increasing rapidly since 1995 (Fig. 1d-e; refs 36,37). Thus, we havereturned to conditions similar to the 1960s, and should expect to see anomalously warm water exported through the compensated mechanism to the UNADW layer of the subtropical Atlantic in the near future. In the longer term, we expect the salinity of the SPG to play a major role in regulating heat uptake into the deep North Atlantic by the compensated mechanism. The evolution of SPG salinity in response to rising levels of greenhouse gases is determined by a competition between a tendency for freshening, due to increases in precipitation (P) minus evaporation (E), and river runoff, at high latitudes (including the Arctic), and an opposite tendency, due to the transport of increasingly saline waters from lower latitudes (where the change in P – E is mostly negative). Models suggest that the results of this competition are time dependent. For example, in projections with the HadCM3 (Hadley Centre Coupled Model, version 3) model SPG salinity declines until the mid-twenty-first century before rising to levels that, by 2100, exceed those simulated for the twentieth century[38]. Our results demonstrate that better understanding this competition, including its interaction with changes in circulation, is a key issue for projections of ocean heat uptake.

Methods

Five-year average temperature and salinity climatologies at $1 \times 1^{\circ}$ horizontal Q8 resolution and 10 m/200 m vertical resolution in the North Atlantic were constructed using the Hydrobase[39] software package and data base, following and expanding on the method used in ref. 40. The gridding was performed along isopycnals, aiding the characterization and preservation of water mass properties, which is key to our analysis. The pentads used range from (1953–1957) to (2003–2007). There are many sources of errors in such an analysis: instrumental errors, interdependency between stations as they typically are obtained along cruise tracks, the interpolation methods and so on. The largest error is however most likely stemming from the undersampling in each region in each pentad. To quantify this error we created a large set of climatologies based on randomly subsampling the original data set by 50% to estimate the span in likely outcomes at a 90% confidence level. Analysing temperature and salinity changes in water masses that are themselves defined by temperature and salinity is obviously a challenge. Heat content change can be calculated only within fixed volumes, but within the water masses both volume and temperature change. By separating these effects a clearer picture emerges. The separation is made in three ways. First, we use the 50-year average positions of the water mass interfaces as the upper and lower limit of the water masses. This allows us to look at heat content changes, because the volumes are fixed. Second, we allow, more realistically, the positions of the water mass interfaces to vary as a function of time. In that case we cannot formally look at heat content change, because the volume is changing, but we can look at temperature anomalies and make inferences about signal propagation. Finally, we make a formal separation of the two effects by defining what we call QHC. This separation allows us to quantify the effects of volume change and thereby make inferences about short-term (seasonal to decadal) and long-term (decadal to century scale) heat uptake in the deep ocean.

Further information on the methods used in this paper can be found in the Supplementary Information. The data can be found at http://www.whoi.edu/science/PO/hydrobase; see also refs 39,41.

Acknowledgements

C.M. and A.M. acknowledge the support of the Norwegian Research Council through iAOOS-Norway (grant number 176096) and the European Union through its 6^{th} Framework Programme Integrated Project DAMOCLES. R.T.S. acknowledges the support of the UK National Centre for Atmospheric Science and the Natural Environment Research Council. We thank J. Gregory and R. Tailleux for valuable comments on the manuscript. We thank R.G. Curry for providing the new Atlantic Ocean analyses, and for valuable assistance with the data analysis at the initial stages of the project.

References

1. Levitus, S., Antonov, J. & Boyer, T. Warming of the world ocean, 1955–2003. *Geophys. Res. Lett.* **32**, L02604 (2005).
2. Bindoff, N.L. et al. in *IPCC Climate Change 2007: The Physical Science Basis* (eds Solomon, S. *et al.*) (Cambridge Univ. Press, 2007).
3. Domingues, C.M *et al.* Improved estimates of upper-ocean warming and multi-decadal sea-level rise. *Nature* **453**, 1090–1093 (2008).
4. Ishii, M. & Kimoto, M. Reevaluation of historical ocean heat content variations with time-varying XBT and MBT depth bias corrections. *J. Oceanograph.* **65**, 287–299 (2009). Q10
5. Levitus, S. *et al.* Global ocean heat content 1955–2008 in light of recently revealed instrumentation problems. *Geophys. Res. Lett.* **36**, L07608 (2009).
6. Purkey, S. & Johnson, G. Warming of global abyssal and deep southern ocean waters between the 1990s and 2000s: Contributions to global heat and level rise budgets. *J. Clim.* **23**, 6336–6351 (2010).
7. Song, Y. & Colberg, F. Deep ocean warming assessed from altimeters, gravity recovery and climate experiment, in situ measurements, and a non-Boussinesq ocean general circulation model. *J. Geophys. Res.* **116**, C02020 (2011).
8. Trenberth, K. Global change: The ocean is warming, isn't it? *Nature* **465**, 304 (2010).
9. Lozier, M.S. *et al.* The spatial pattern and mechanisms of heat-content change in the North Atlantic. *Science* **319**, 800–803 (2008).
10. Ganachaud, A. & Wunsch, C. Large-scale ocean heat and freshwater transports during the World Ocean Circulation Experiment. *J. Clim.* **16**, 696–705 (2003).
11. Lumpkin, R. & Speer, K. Global ocean meridional overturning. *J. Phys. Oceanograph.* **37**, 2550–2562 (2007).
12. Talley, L. Freshwater transport estimates and the global overturning circulation: shallow, deep and throughflow components. *Prog. Oceanograph.* **78**, 257–303 (2008).
13. Dickson, R. *et al.* Long-term coordinated changes in the convective activity of the North Atlantic. *Prog. Oceanograph.* **38**, 241295 (1996).
14. Curry, R.G. & McCartney, M.S. Ocean gyre circulation changes associated with the North Atlantic Oscillation. *J. Phys. Oceanograph.* **31**, 3374–3400 (2001).
15. Visbeck, M. *et al.* The ocean's response to North Atlantic Oscillation variability. In *The North Atlantic Oscillation: Climatic Significance and Environmental Impacts* Vol. 134 (eds Hurrell, J.W., Kushnir, J.W., Ottersen, Y. Visbeck, G.) (Geophysical Monograph Series, American Geophysical Union, 2003).
16. Munk, W. & Wunsch, C. Abyssal recipes II: energetics of tidal and wind mixing. *Deep-Sea Res.* **45**, 1977–2010 (1998).
17. Bindoff, N.L. McDougall, T.J. Diagnosing climate change and ocean ventilation using hydrographic data. *J. Phys. Oceanograph.* **24**, 1137–1152 (1994).
18. Curry, R.G. *et al.* Oceanic transport of subpolar climate signals to mid-depth subtropical waters. *Nature* **391**, 575–577 (1998).
19. Yashayaev, I., van Aken, H.M., Holliday, N.P. & Bersch, M. Transformation of the Labrador Sea Water in the subpolar North Atlantic. *Geophys. Res. Lett.* **34**, L22605 (2007).
20. Yashayaev, I. & Clarke, A. Evolution of North Atlantic water masses inferred from Labrador Sea salinity series. *Oceanography* **21**, 30–45 (2008).
21. Johnson, G.C. & Wijffels, S.E. Ocean density change contributions to sea level rise. *Oceanography* **24**, 112–121 (2011).
22. Lozier, M.S. *et al.* Opposing decadal changes for the North Atlantic meridional overturning circulation. *Nature Geosci.* **3**, 728–734 (2010).
23. Levitus, S., Antonov, J.I., Boyer, T.P. & Stephens, C. Warming of the world ocean. *Science* **287**, 2225–2229 (2000).
24. Yashayaev, I. Hydrographic changes in the Labrador Sea, 1960–2005. *Prog. Oceanograph.* **73**, 242–276 (2007).
25. Sarafanov, A. On the effect of the North Atlantic Oscillation on the temperature and salinity of the subpolar North Atlantic intermediate and deep waters. *ICES J. Mar. Sci.* **66**, 1448–1454 (2009).
26. Talley, L.D. & McCartney, M.S. Distribution and circulation of Labrador Sea Water. *J. Phys. Oceanograph.* **12**, 1189–1205 (1982).
27. Fine, R.A. & Molinary, R.L. A continuous deep western boundary Current between Abaco (26.5°N) and Barbados (13°N). *Deep-Sea Res. A* **35**, 1441–1450 (1988).
28. Sebille, E.v. *et al.* Propagation pathways of classical Labrador Sea Water from its source region to 26°N. *J. Geophys. Res.* **116**, C12027 (2011).
29. Leadbetter, S.J., Williams, R.G., McDonagh, E.L & King, B.A. A twenty year reversal in water mass trends in the subtropical North Atlantic. *Geophys. Res. 52 Lett.* **34**, L12608 (2007).
30. Rhein, M. The Deep Western Boundary Current: Tracers and velocities. *Deep-Sea Res. I* **41**, 263–281 (1994).
31. Robson, J., Sutton, R., Lohmann, K., Smith, D. & Palmer, M.D. Causes of the 54 rapid warming of the North Atlantic Ocean in the Mid-1990s. *J. Clim.* **25**, 4116–4134 (2012).
32. Koltermann, K.P. *et al.* Decadal changes in the thermohaline circulation of the North Atlantic. *Deep-Sea Res. II* **46**, 109–138 (1999).
33. Bower, A., Lozier, M., Gary, S. Boning, C. Interior pathways of the North Atlantic meridional overturning circulation. *Nature* **459**, 243–247 (2009).
34. Drinkwater, K. The regime shift of the 1920s and 1930s in the North Atlantic. *Prog. Oceanograph.* **68**, 134–151 (2006).
35. Johnson, G., Purkey, S. Toole, J. Reduced Antarctic meridional overturning circulation reaches the North Atlantic Ocean. *Geophys. Res. Lett.* **35**, L22601 (2008).
36. Holliday, N.P. *et al.* Reversal of the 1960s to 1990s freshening trend in the northeast North Atlantic and Nordic Seas. *Geophys. Res. Lett.* **35**, L03614 (2008).
37. Hughes, S.L., Holliday, N.P. & Beszczynska-Mller, A. ICES Report on Ocean Climate 2009. *ICES Cooperative Research Report*, **304**, 67pp (2010).
38. Stott, P.A., Sutton, R.T. & Smith, D.M. Detection and attribution of Atlantic salinity changes. *Geophys. Res. Lett.* **35**, L21702 (2008).
39. Lozier, M.S., Owens, W.B. & Curry, R.G. The climatology of the North Atlantic. *Prog. Oceanograph.* **36**, 1–44 (1995).
40. Curry, R. & Mauritzen, C. Dilution of the northern North Atlantic Ocean in recent decades. *Science* **308**, 1772–1774 (2005).
41. Curry, R. HydroBase 2: A database of hydrographic profiles and tools for climatological analysis. Available from http://www.whoi.edu/science/PO/hydrobase. 81pp (2001).
42. Hurrell, J.W. & Deser, C. North Atlantic climate variability: The role of the North Atlantic Oscillation. *J. Mar. Syst.* **79**, 231–244 (2010).

Supplementary information

Data and gridding

5-year average climatologies for the North Atlantic Ocean were constructed using the HydroBase2[S1] software package and database. Using isopycnal gridding and interpolating techniques, 3-D fields of salinity, potential temperature, and potential density were generated by an iterative algorithm for non-overlapping 5-year time frames spanning the years 1953–2007. The method used here follows the method used in [S2], with two key exceptions: there is an intermediate step added to the process, namely 15-year climatologies, and there is one additional 5-year climatology, namely 2003-2007.

The resolution is 1° in latitude and longitude and 10 m/ 200 m in the vertical. The region considered is 20°N to 66°N/ the Greenland-Scotland Ridge.

The iterative procedure was performed as follows: Initially, a 51 year (1955-2005) gridded climatology was created based on all relevant HydroBase data. This climatology was subsequently used as a basis for interpolation to grid cells with missing values. Then, we created 4 fifteen-year climatologies, and finally 11 five-year climatologies. This 3-step iterative procedure, which was developed after the [S2] study, reduces the gaps in the data record and retains more information of the temporal variability in the dataset.

The details of the production of the set of 15 year climatologies are:

1. A preliminary 15 year annual-mean climatology with a resolution of 1° for depths below 200 m was constructed by gridding all profile data from the given period. At grid cells with missing values, the differences between property values of the 15 year climatology and the 51 year climatology were interpolated. The mapping uses distance-weights along isopycnal surfaces from the 51 year climatology fields, assuming a Gaussian correlation function with a 200 km length scale. The search area is further restricted horizontally by a search radius of 5°.
2. Then, monthly-mean climatologies for each of the 4 fifteen year periods were produced by gridding a set of hybrid profiles consisting of all observed profiles from the relevant month, plus the profiles from the corresponding, regularly spaced, annual-mean climatology described above. Recall that the latter product only has values beneath 200 m, in order to have a minimal impact on the seasonal cycle in this gridded monthly-mean product. Missing data were filled as described above; note here that the filling algorithm has a special treatment for missing values in the mixed layer.
3. All 12 monthly-mean climatologies were merged into a gridded annual-mean product, and again, any missing values were filled using the 51 year climatology as outlined above. The final version of the 4 fifteen year climatologies was then produced by applying a two-dimensional Laplacian smoother along isopycnal surfaces, using a smoothing radius of 1°.

The pentadal climatologies were produced by the same algorithm, for 5 year periods starting with the 1953-57 period and ending with the 2003-2007 period. At this stage, the 51 year climatology was replaced by the 15 year climatologies.

Definition of Regions

- Extratropical North Atlantic: Bounded in south by the 20°N latitude line, and in the north by 66°N west of Greenland, and the Greenland-Scotland Ridge east of Greenland. The Caribbean and the Mediterranean Seas are not included.
- Subtropical North Atlantic: between 20°N and 50°N, excluding the Caribbean and the Mediterranean Seas.
- Subpolar North Atlantic: Bounded in south by the 50°N latitude line, and in the north by 66°N west of Greenland, and the Greenland-Scotland Ridge east of Greenland.

Error Analysis

Despite the unusually high density of hydrographic data in the North Atlantic Ocean, the region is still formally undersampled in terms of the analysis we perform here. In particular, the analysis of the Lower North Atlantic Deep Water and the modified Antarctic Bottom Water suffers from a lack of data, as indicated in Suppl. Fig. 1, which shows the position and vertical extent of hydrographic profiles for the most, and least, sampled pentads.

We made quantitative estimates of the uncertainties associated with undersampling based on 32 sub-samples of the full data set. The full data set was organized into regions that span 10° in longitude and 10° in latitude (Marsden Squares) and into one year time slots. Each sub-sampled data set was constructed by drawing 50% of the profiles randomly from each Marsden Square and each year, without replacement. Hence, the relative distribution, geographically and temporally, of the full data set was retained in each sub-sample.

Following the method that was described in *Data and gridding* above and used to construct the eleven pentadal climatologies, we constructed a total of 11 times 32 sub-sampled pentadal climatologies. Error estimates were defined by first discarding the lowest and highest value in each pentad and then estimating the interval spanned by the 30 remaining values. This span gives an estimate of the 90% confidence interval with a normal distribution. Note that with 32 sub-sampled datasets the size of this confidence interval itself has a 15% uncertainty. The results from the error analysis are given in Suppl. Tbl. 3.

Error estimates associated with our calculations of net changes from 1955 to 2005 are based on the error estimates for the first and the last pentads. (Generally, error estimates are largest for the initial pentad; see, e.g., table S1.) Error estimates associated with the pentadal water mass analysis are given in Suppl. Fig. 2.

These estimates do not describe the full range of errors. First of all, more sub-samples should have been used. However, the construction of the 5 year sub-sampled climatologies was computationally demanding, making it difficult with the resources at hand to expand beyond the 352 sub-sampled data sets that our error estimates are based on.

Secondly, our estimates will be affected by the use of climatological values in regions where observations were lacking, by inter-dependencies between hydrographic stations and by the gridding method. Finally, observations are typically sampled along cruise tracks, and not uniformly in the ocean. This limits the number of degrees of freedom in the data, which affects our error estimates.

We have additional confidence in our results by the very fact that the signals are large compared to the background noise (and consistent with simple geophysical hypotheses about deep ocean circulation).

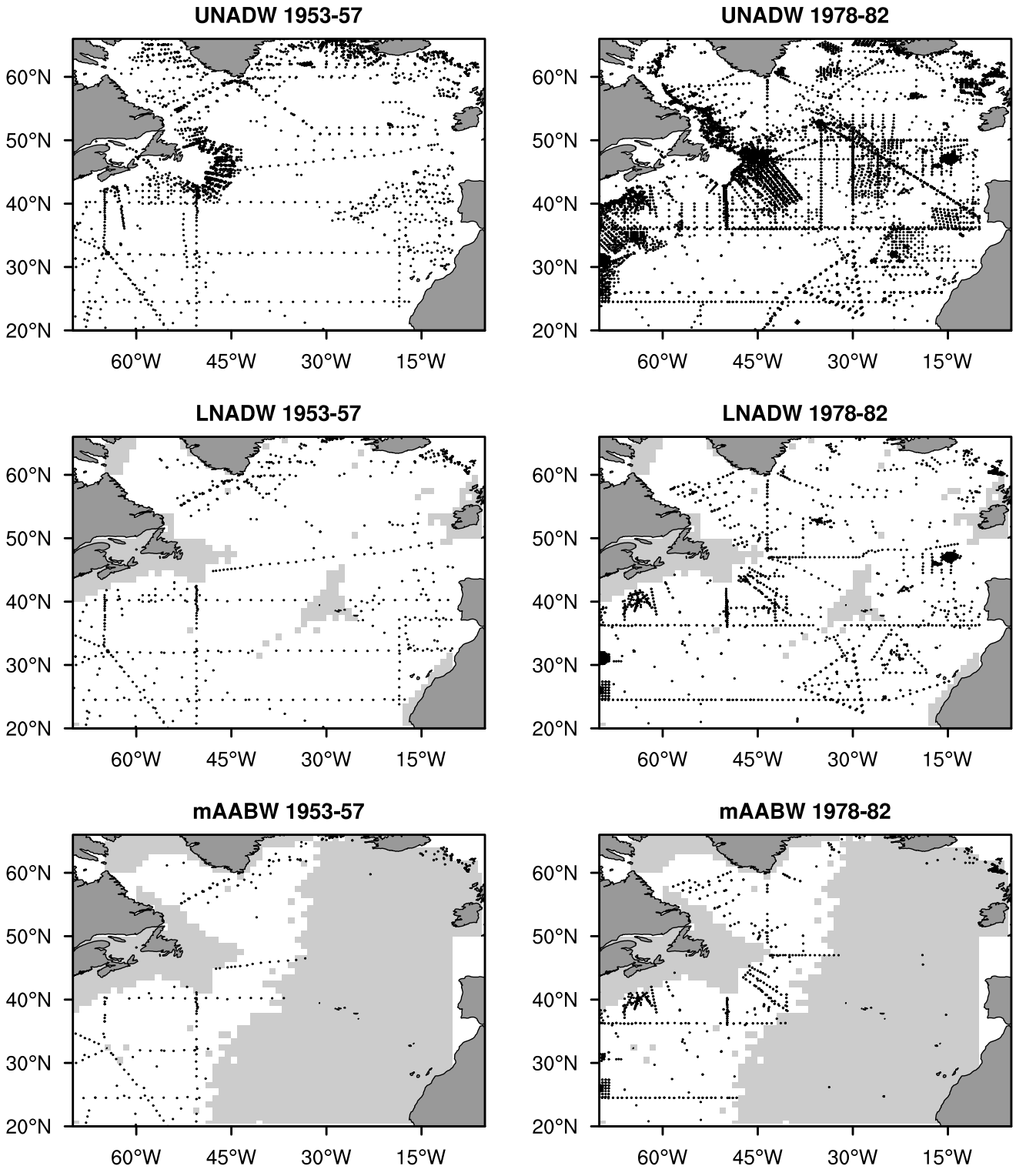

Supplementary Figure 1: Position of profiles with hydrography data used in the present study. Displayed in the left and the right columns of panels are positions for the pentads 1953-57 and 1978-82, respectively. These are the pentads with the lowest and highest number of profiles in LNADW, respectively. Light grey shading shows regions over which the control volumes do not extend.

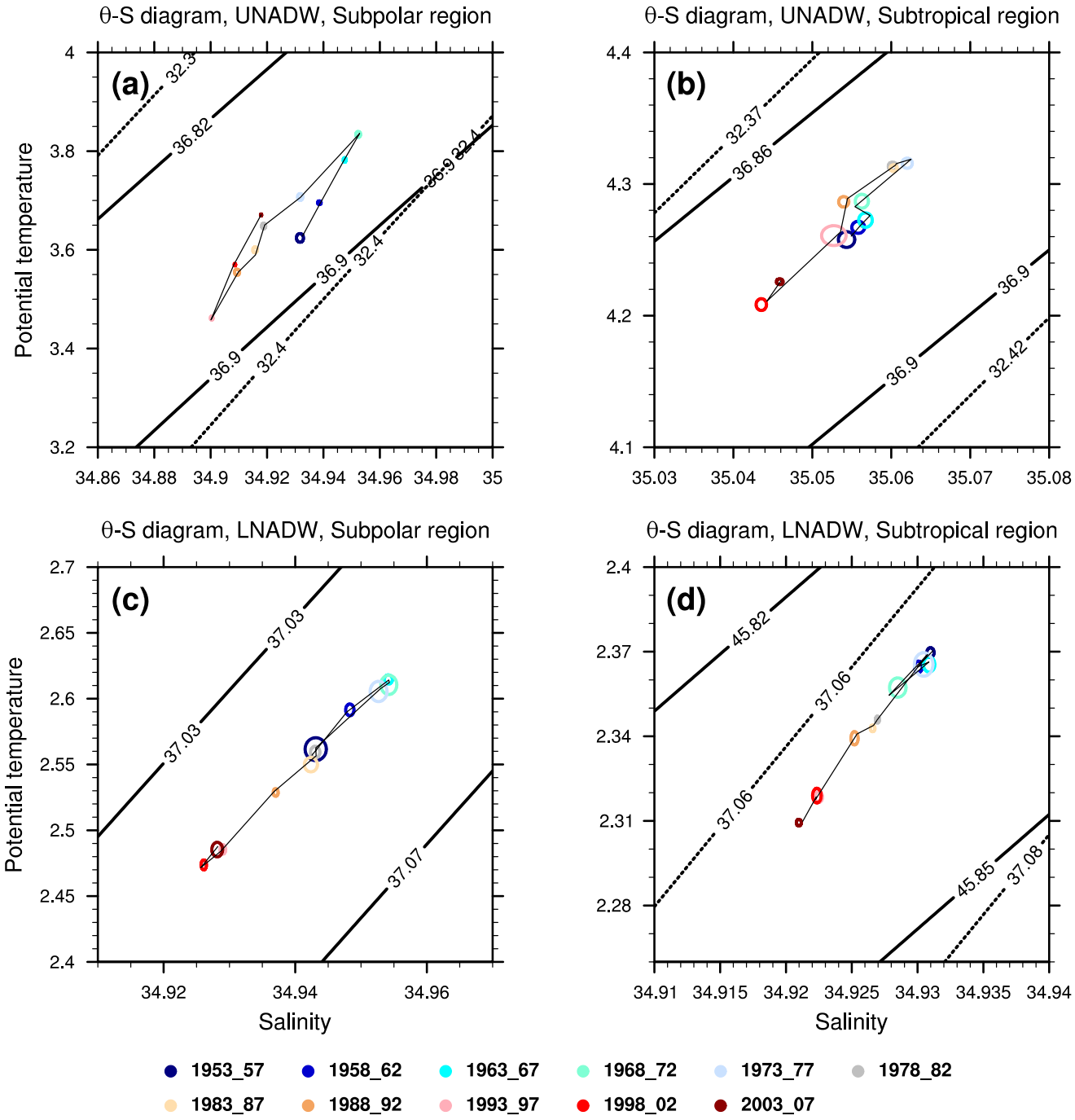

Supplementary Figure 2: Average water mass properties for the water masses UNADW (a,b) and LNADW(c,d), in the Subpolar (a,c) and Suptropical (b,d) regions and for each pentad used in the analysis (color coded). The size of the circles indicates the error associated with undersampling. The circles are centered on the mean values of the 32 sub-sampled data sets, and the horizonta l and vertical radii have been set to the sub-samples' standard deviations of salinity and potential temperature, respectively. The labelled thick black lines show selected isopleths for density. For water masses which are limited by isopycnals at different reference pressure levels, dashed lines and full lines correspond to the upper and lower references levels, respectively. The instrumental errors (see e.g.[S3]) are typically much smaller than these errors. Note however one key exception: the instrument errors dominate in the LNADW in the Subtropical Gyre during the first pentad.

Alternative decomposition of heat content within water masses: Quasi-Heat Content (QHC)

We introduce the following quantities:

H	is quasi-heat content (QHC) per unit area
z^b, z^t	are the levels at the bottom and top of the layer, respectively ($z^b > z^t$)
$_r$	(subscript) denotes a reference quantity
$T(z), T_r(z)$	are profiles of pentadal potential temperature and reference potential temperature, respectively

Let $_r$ denote quantities that refer to the 1955-2005 climatology. The QHC anomaly per unit area relative to the climatology is

$$dH = \rho_{ref} c_p \Big[\int_{z^t}^{z^b} T(\zeta) d\zeta - \int_{z_r^t}^{z_r^b} T_r(\zeta) d\zeta \Big] = \rho_{ref} c_p \big[h\overline{T} - h_r \overline{T_r} \big] \tag{1}$$

where

$$\overline{T_{(r)}} \equiv h_{(r)}^{-1} \int_{z_{(r)}^t}^{z_{(r)}^b} T_{(r)}(\zeta) d\zeta \tag{2}$$

i.e., the vertical mean of the (reference) potential temperature in the isopycnal layer. Furthermore, ρ_{ref} is a reference density, c_p is the specific heat capacity, and $h_{(r)}$ is the thickness of the (reference) layer.
The QHC anomaly per unit area that can be attributed to the temperature anomaly relative to $\overline{T_r}$ becomes

$$dH_r = \rho_{ref} c_p \Big[\int_{z^t}^{z^b} [T(\zeta) - \overline{T_r}] d\zeta \Big] = \rho_{ref} c_p h \overline{\Delta T} \tag{3}$$

where $\overline{\Delta T} = \overline{T} - \overline{T_r}$ is the temperature anomaly.
The difference between the anomalies in Eq.s 1 and 3 may then be written:

$$dH^h \equiv dH - dH_r = \rho_{ref} c_p \Big[\int_{z^t}^{z^b} \overline{T_r} d\zeta - \int_{z_r^t}^{z_r^b} T_r(\zeta) d\zeta \Big] = \rho_{ref} c_p \overline{T_r} \Delta h \tag{4}$$

where $\Delta h = h - h_r$ is the anomaly in the thickness of the isopycnal layer.
We note that dH^h represents the QHC anomaly per unit area due to volume changes, since the only time-dependent variable in Eq. 4 is the layer thickness. The interpretation of the expression in Eq. 3 is more subtle, since it involves both time varying temperature and layer thickness. If we define

$$dH^T \equiv \rho_{ref} c_p h_r \overline{\Delta T} \tag{5}$$

we have introduced an expression that can be attributed solely to changes in water mass properties. We may now write

$$dH = dH^T + dH^h + \rho_{ref} c_p \Delta h \overline{\Delta T} \tag{6}$$

Note that $\overline{\Delta T}$ from Eq. 3 is slightly different from the more intuitive definition adopted for climatological water mass interfaces ($\rho_{ref} c_p \int_{z_r^t}^{z_r^b} [T(\zeta) - \overline{T_r}] d\zeta / h_r$). The modification introduced here is due to the requirement that the remainder should be small after the integral was split into contributions from volume changes (dH^h) and temperature changes (dH^T). If anomalies in isopycnal space arise in response to changes in (deep) water formation, the latter term in Eq. 6 will be positive when increases in the volume of a water mass correlate with warm (and salt enriched) anomalies. Conversely, this term will be negative when increases in the volume correlate with cold (and salt deprived) anomalies.

The interpretation of the other terms can be summarized as follows:

dH defined in Eq. 1	is the total QHC anomaly per unit area within the (time-varying) volume that constitutes an isopycnal layer (when z^b and z^t are isopycnal interfaces)
dH^T defined in Eq. 5	represents the QHC anomaly per unit area due to anomalous temperatures
dH^h defined in Eq. 4	represents the QHC anomaly per unit area due to volume changes (positive when the isopycnal volume exceeds the reference volume and $\overline{T_r} > 0$)

References

S1. Curry, R. HydroBase 2: A Database of Hydrographic Profiles and Tools for Climatological Analysis. Available from http://www.whoi.edu/science/PO/hydrobase. 81 pp (2001)

S2. Curry, R. & Mauritzen, C. Dilution of the northern North Atlantic in recent decades. *Science*, **308**, 1772-1774 (2005).

S3. Gouretski V. & Jancke, K. A consistent pre-WOCE hydrographic data set for the south Atlantic: Station data and gridded fields. WOCE Report No. 127/95, Hamburg, Germany, 32 pp.

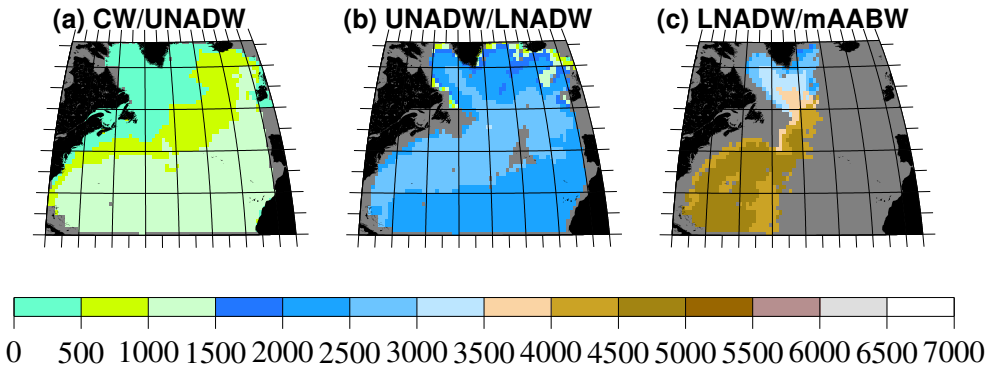

Supplementary Figure 3: Average (1955-2005 mean) depth [m] of lower interface of the water masses (a) Central Waters, (b) Upper North Atlantic Deep Water and (c) Lower North Atlantic Deep Water. Grey shading shows regions where the interface is not found in the gridded product.

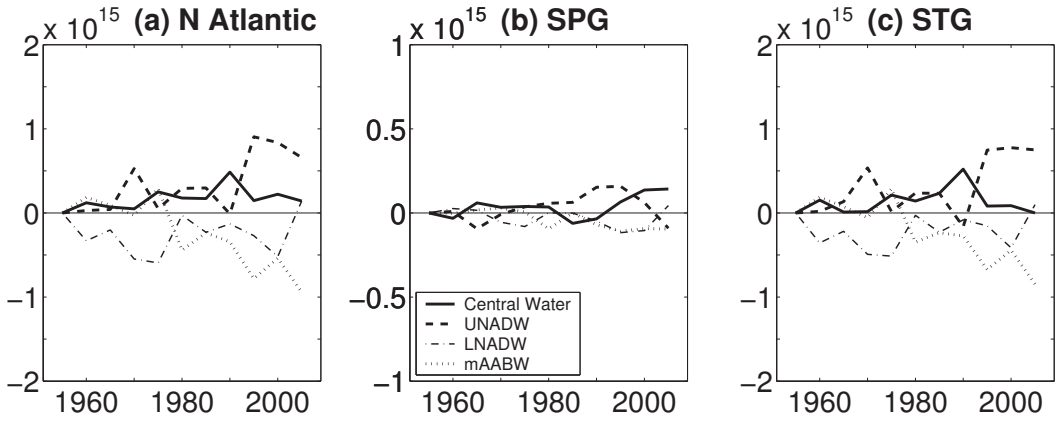

Supplementary Figure 4: Volume change [m^3] within the water masses defined in Suppl. Tbl. 2, calculated between the "instantaneous" (5-year average) position of each water mass interface, for a) the extratropical North Atlantic Ocean (20°N-66°N/Greenland-Scotland Ridge; b) Subpolar Gyre (50°N-66°N/Greenland-Scotland Ridge) and c) the Subtropical Gyre (20°N-50°N). Anomalies are offsets from the 1953-1957 pentad. The uncertainties are given in Suppl. Tbl. 3.

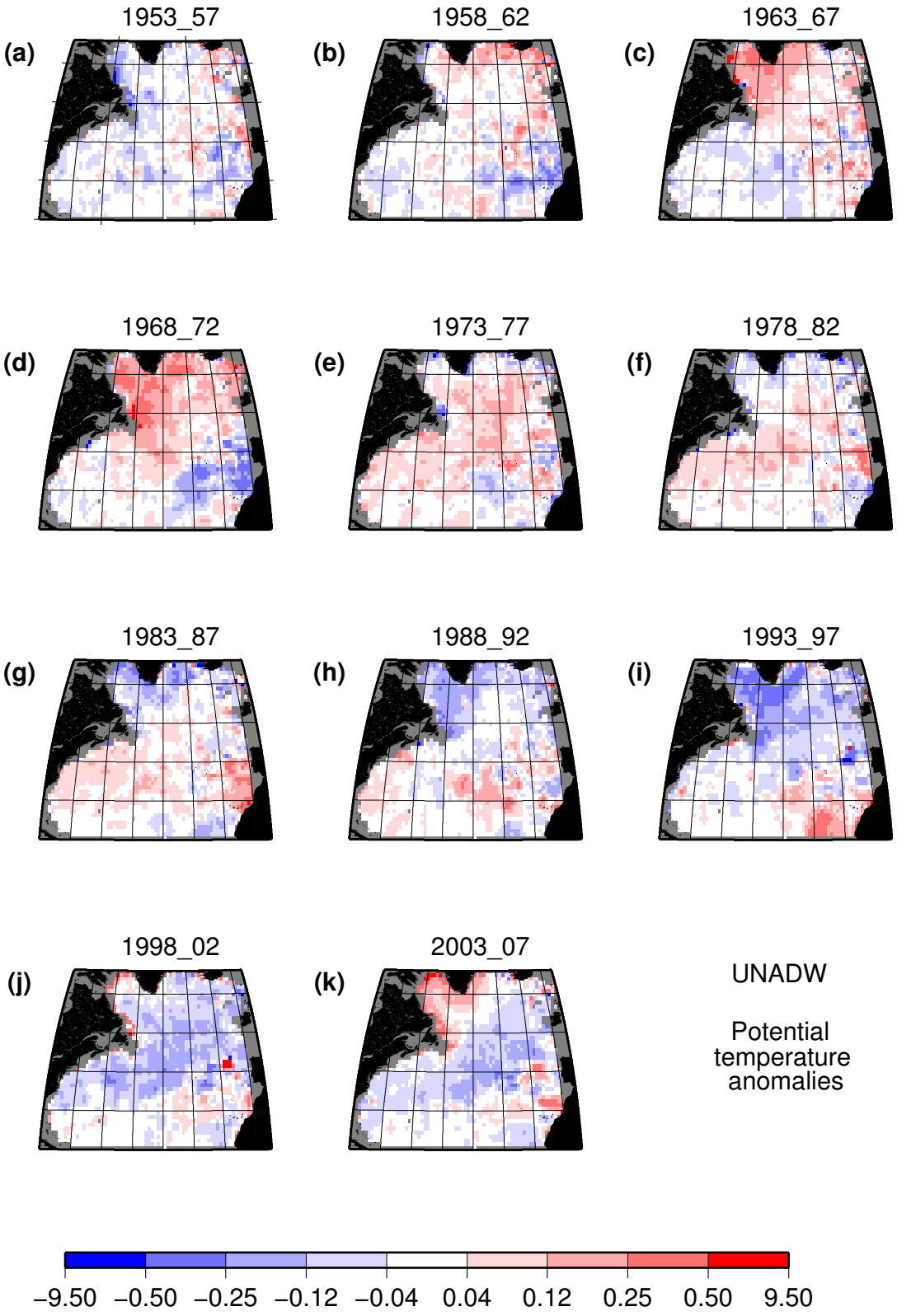

Supplementary Figure 5: Maps of potential temperature anomalies in the Upper North Atlantic Deep Water (UNADW) for each of the 11 pentads in this study (years are displayed in the panel titles). Anomalies are relative to the average of the full time series displayed. Grey shading shows regions where UNADW data are missing.

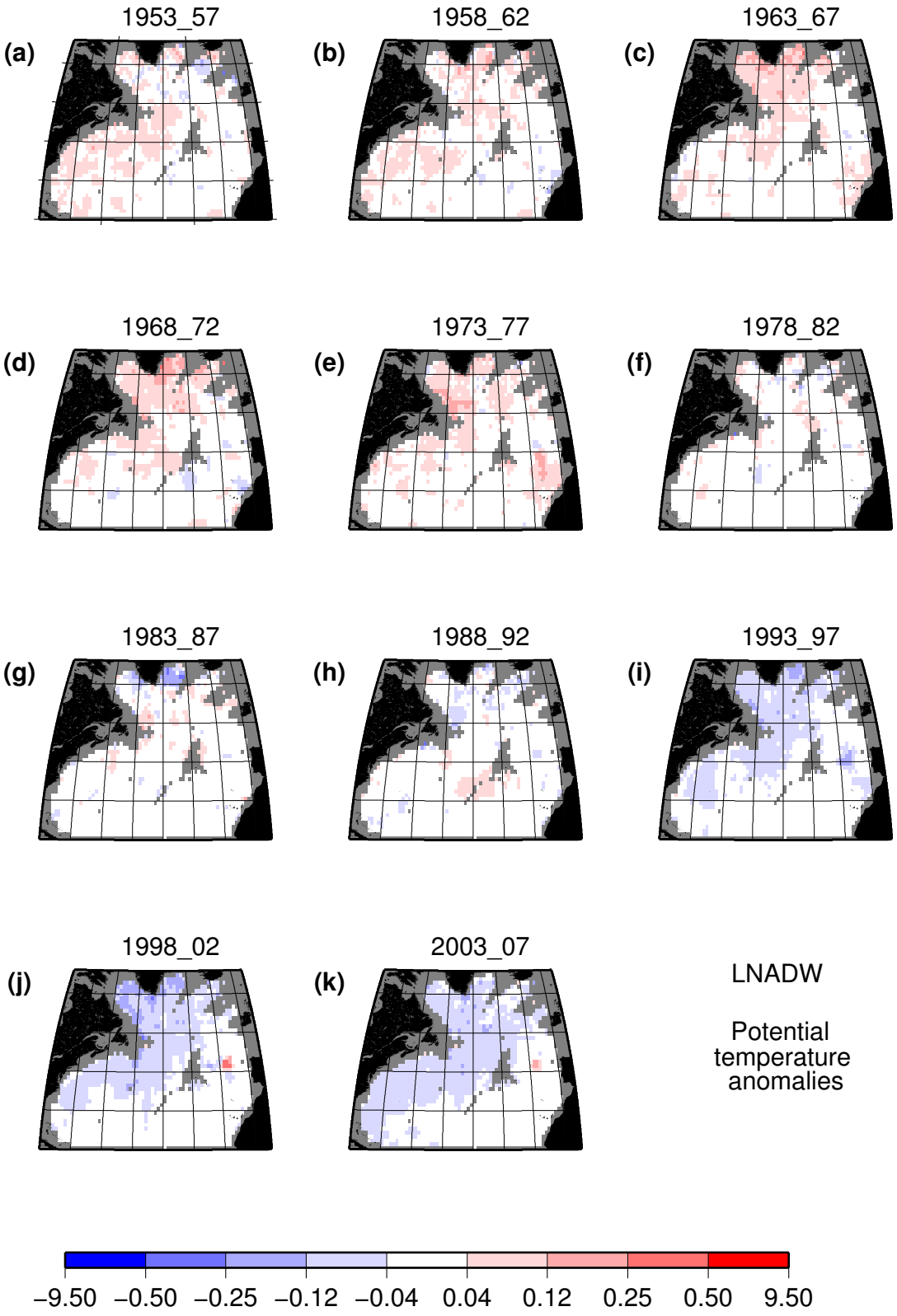

Supplementary Figure 6: As Suppl. Fig. 5, but for the Lower North Atlantic Deep Water (LNADW).

	0-700 m	700-2000 m	2000 m-bottom	Total
(a) Subtropical Gyre				
1953-57	-1.4 ±2.7	-5.2 ±1.7	1.3 ±0.6	-5.3 ±4.5
1958-62	-4.0 ±1.5	-2.5 ±1.6	0.9 ±0.5	-5.7 ±2.7
1963-67	-9.3 ±1.3	-2.9 ±1.5	1.4 ±0.6	-10.8 ±2.7
1968-72	-8.7 ±1.2	-3.5 ±1.4	2.1 ±0.7	-10.1 ±3.0
1973-77	-2.0 ±0.9	3.6 ±1.2	2.2 ±1.0	3.8 ±2.2
1978-82	-3.5 ±1.3	2.9 ±1.2	1.4 ±0.5	0.8 ±2.0
1983-87	-2.1 ±0.9	3.9 ±0.9	1.1 ±0.3	2.9 ±1.7
1988-92	2.2 ±1.0	8.5 ±1.1	-0.5 ±0.5	10.2 ±2.5
1993-97	6.4 ±1.6	1.8 ±1.5	-1.9 ±0.4	6.3 ±2.2
1998-02	10.9 ±1.4	-2.7 ±1.4	-3.8 ±0.3	4.5 ±2.1
2003-07	11.5 ±0.8	-3.8 ±0.6	-4.3 ±0.3	3.4 ±1.3
(b) Subpolar Gyre				
1953-57	-0.4 ±0.6	-0.3 ±0.3	-0.1 ±0.3	-0.7 ±0.9
1958-62	1.4 ±0.3	0.8 ±0.2	0.3 ±0.1	2.5 ±0.4
1963-67	3.1 ±0.4	2.0 ±0.2	0.7 ±0.1	5.8 ±0.6
1968-72	1.0 ±0.5	3.7 ±0.3	0.9 ±0.2	5.6 ±1.0
1973-77	-2.2 ±0.3	1.3 ±0.3	0.8 ±0.2	-0.0 ±0.4
1978-82	-2.6 ±0.3	0.3 ±0.2	0.5 ±0.1	-1.6 ±0.6
1983-87	-4.9 ±0.3	-1.7 ±0.2	-0.0 ±0.2	-6.6 ±0.6
1988-92	-4.4 ±0.3	-2.3 ±0.2	0.0 ±0.1	-6.7 ±0.5
1993-97	-0.5 ±0.6	-3.5 ±0.3	-0.8 ±0.1	-4.7 ±0.9
1998-02	3.7 ±0.3	-1.1 ±0.2	-1.2 ±0.2	1.4 ±0.4
2003-07	5.7 ±0.1	0.7 ±0.2	-1.2 ±0.1	5.1 ±0.3
(c) Total				
1953-57	-1.8 ±2.7	-5.5 ±1.7	1.3 ±0.7	-6.1 ±5.0
1958-62	-2.6 ±1.5	-1.7 ±1.5	1.2 ±0.5	-3.2 ±2.8
1963-67	-6.2 ±1.5	-0.9 ±1.4	2.2 ±0.6	-5.0 ±2.7
1968-72	-7.7 ±1.2	0.2 ±1.3	3.0 ±0.7	-4.5 ±2.8
1973-77	-4.2 ±1.1	4.9 ±1.4	3.0 ±1.1	3.7 ±2.3
1978-82	-6.1 ±1.4	3.2 ±1.1	2.0 ±0.4	-0.8 ±1.9
1983-87	-7.0 ±0.8	2.2 ±0.8	1.1 ±0.4	-3.7 ±1.5
1988-92	-2.2 ±1.2	6.2 ±1.2	-0.5 ±0.5	3.5 ±2.4
1993-97	5.9 ±1.5	-1.7 ±1.5	-2.7 ±0.5	1.6 ±2.5
1998-02	14.6 ±1.5	-3.8 ±1.4	-5.0 ±0.3	5.9 ±2.5
2003-07	17.2 ±0.9	-3.1 ±0.7	-5.5 ±0.3	8.5 ±1.3

Supplementary Table 1: Heat content anomalies [10^{21} J] in depth space, relative to the mean of each time series. (a) The Subtropical Gyre, defined as the region between 20°N and 50°N; (b) the Subpolar Gyre, the domain between 50°N and the Greenland-Scotland Ridge in the northeast and the Labrador Sea (south of 66°N) in the northwest; and (c) the sum of the two.

	Upper density/ typical depth	Lower density/ typical depth	Comments
Central Waters (CW)	Sea Surface	σ_1=32.15/ 100m (SPG) - 1200m (STG)	Includes Mediterranean outflow waters, which give rise to a salt water tongue at roughly 1000 meters extending westward from the Strait of Gibraltar, and Antarctic Intermediate water, also at about 1000m, giving rise to a freshwater tongue originating in the southwest of the domain.
Upper North Atlantic Deep Water (UNADW)	σ_1=32.15/ 100m (SPG) - 1200m (STG)	σ_2=37.0/ 1500m (SPG) - 3000m (STG)	
Lower North Atlantic Deep Water (LNADW)	σ_2=37.0/ 1500m (SPG) - 3000m (STG)	σ_2=37.1 (SPG), σ_4=45.9 (STG)/ 2000m (SPG) - 4500m (STG)	Includes entrained water.
Modified Antarctic Bottom Water (mAABW)	σ_2=37.1 (SPG), σ_4=45.9 (STG)/ 2000m (SPG) - 4500m (STG)	Ocean bottom	

Supplementary Table 2: Characteristics of water masses used in the analysis.

Figure 1							
	10^{21} J		10^{21} J			10^{13} kg	
	a		**b**	**c**	**d**	**e**	**f**
Line label		*Line label*					
0m-700m	1.4	Central Water	1.8	1.8	0.3	1.6	1.2
700m-2000m	1.3	UNADW	0.9	0.9	0.3	0.9	0.9
2000m-bottom	0.4	LNADW	0.4	0.4	0.1	1.1	1.2
		mAABW	0.1	0.1	0.1	1.5	1.7
0m-bottom	2.5	Total	2.5	2.5	0.6	2.9	2.9

Figure 3				
	10^{21} J			
	a	**b**	**c**	**d**
Line label				
temp. change	1.3	0.8	0.4	0.06
vol. change	2.7	2.0	1.6	1.0
cross-term	0.1	0.1	0.05	0.02
layer total	2.9	1.8	1.6	1.0

Figure S4			
	10^{14} m^3		
	a	**b**	**c**
Line label			
Central Water	0.6	0.2	0.5
UNADW	1.2	0.5	1.1
LNADW	1.8	0.5	1.7
mAABW	1.4	0.3	1.4

Supplementary Table 3: Error estimates for Figures 1, 3, and S4. Thirtytwo sub-sampled sets were constructed by drawing 50% of the profiles randomly from each yearly file, without replacement. We first discarded the lowest and highest values, so the tabulated error estimates correspond to the intervals spanned by the 30 remaining values. See **Error Analysis** above for details.